

FAST: A Fully Asynchronous Split Time-Integrator for Self-Gravitating Fluid

Takayuki R. SAITOH¹ and Junichiro MAKINO^{1,2,3}

¹ *Division of Theoretical Astronomy, National Astronomical Observatory of Japan, 2–21–1 Osawa, Mitaka-shi, Tokyo 181–8588.*

² *Center for Computational Astrophysics, National Astronomical Observatory of Japan, 2–21–1 Osawa, Mitaka-shi, Tokyo 181–8588*

³ *Department of Astronomical Science, School of Physical Sciences, The Graduate University for Advanced Studies (SOKENDAI), 2–21–1 Osawa, Mitaka-shi, Tokyo 181–8588, Japan.
saitoh.takayuki@nao.ac.jp, saitoh.takayuki@cfca.jp*

(Received 2009 August 10; accepted 200 0)

Abstract

We describe a new algorithm for the integration of self-gravitating hydrodynamical systems using SPH method. We split the Hamiltonian of a self-gravitating fluid system to the gravitational potential and others (kinetic and internal energies) and use different time-steps for their integrations. The time integration is done in the way similar to that used in the mixed variable symplectic or multiple stepsize symplectic schemes. We performed three test calculations. One was the spherical collapse and the other was an explosion. We also performed a realistic test, in which the initial model was taken from a simulation of merging galaxies. In all test calculations, we found that the number of time-steps for gravitational interaction were reduced by nearly an order of magnitude when we adopted our integration method. In the case of the realistic test, in which the dark matter potential dominates the total system, the total calculation time was significantly reduced. Simulation results were almost the same with those of simulations with the ordinary individual time-step method. Our new method achieves good performance without sacrificing the accuracy of the time integration.

Key words: galaxies:starburst — galaxies:ISM — ISM:structure — method:numerical

1. Introduction

The number of particles used in simulations of galaxy formation with N -body/Smoothed Particle Hydrodynamics (SPH) method has not increased much since the early days of Katz & Gunn (1991) and Navarro & Benz (1991), though the number of particles used in pure N -body cosmological simulations has increased drastically. For N -body simulations, the largest run in 1991 used $\sim 2 \times 10^6$ particles (Suto & Sugihara 1991) and the largest run recently performed used $\sim 7 \times 10^{10}$ particles (Kim et al. 2008). The number of particles has grown by nearly four orders of magnitudes in two decades. On the other hand, for N -body/SPH simulations of galaxy formation, the first simulations used ~ 4000 SPH particles for a single halo (Katz & Gunn 1991) and the largest simulation which is performed recently used $\sim 3.2 \times 10^5$ SPH particles for a single halo (Governato et al. 2009).¹ The scale up factor is only 80 in two decades. This is because time-steps become quite short in dense and compact self-gravitating gas clouds of star-forming regions.

This problem is severer in simulations with higher resolution, since these simulations resolve denser gas. In gen-

eral, supernova (SN) explosion in dense regions leads the shortest time-step. Here we estimate the decrease of the time-steps due to SNe. We consider a compact region of the interstellar medium (ISM) with the temperature of T_{ISM} , where the sound speed is c_{ISM} , as a potential site of the star formation and that the region is rapidly heated to T_{SN} , where the sound speed is c_{SN} , by SN with the energy of E_{SN} . The ratio between the time-step of the ISM before the SN, dt_{ISM} , and after the SN, dt_{SN} , in the compact region is

$$\begin{aligned} dt_{\text{ISM}}/dt_{\text{SN}} &= c_{\text{SN}}/c_{\text{ISM}}, \\ &\propto (T_{\text{SN}}/T_{\text{ISM}})^{1/2}, \\ &\propto E_{\text{SN}}^{1/2} m^{-1/2} T_{\text{ISM}}^{-1/2}, \end{aligned} \quad (1)$$

where E_{SN} is the energy of the single SN and m is the mass of the heated region or the mass resolution in Lagrange schemes such as SPH, respectively, and we use $T_{\text{SN}} \propto E_{\text{SN}}/m$. From this equation, we can easily find that the time-step ratio becomes larger when (i) mass resolution becomes higher and (ii) the temperature of the ISM becomes lower (see also section 2 for more detailed discussion). Thus high-resolution simulations which model the ISM with low temperature ($< 10^4$ K) require much shorter time-steps than conventional simulations of galaxy formation with a cooling cut off at $\sim 10^4$ K.

The individual time-step method (Aarseth 1963;

¹ Note that a part of SPH particles were converted into star particles, thus the number of SPH particles was reduced during the galaxy evolution.

McMillan 1986; Makino 1991a) reduces the total calculation cost significantly, by assigning different time-steps to different particles and integrating only a small fraction of particles with small time-steps. However, the reduction in the computing time is rather limited, when the individual time-step is used with the tree method (Barnes & Hut 1986). Most of N -body/SPH codes use the tree method for the calculation of gravitational interaction. In these codes, the tree structure is constructed from scratch at every step. The construction cost of tree structure is small compared to the cost of force calculation. However, once we combine the tree method with the individual time-step method, the relative cost of tree construction becomes much higher. The individual time-step is efficient only when the number of particles with small time-steps is small, compared to the total number of particles. In this case, unfortunately, the cost of the tree construction dominates the total cost, because it is independent of the number of particles with small time-steps. Consequently, total performance of simulation is not much improved. Table 1 of Wadsley et al. (2004) showed such a bad case. We can see that a half of the smallest step cost is that of the “Tree building” part.

Several ways to reduce the cost of the tree construction have been reported. McMillan & Aarseth (1993) applied the local update to the tree structure around particles which were updated, instead of reconstructing the whole tree structure at each step. The dynamic updates technique was used in *GADGET-1/2* (Springel et al. 2001; Springel 2005). In *VINE* (Wetzstein et al. 2008; Nelson et al. 2008), the construction frequency of tree structure was reduced by skipping several continuous time-steps and reused old tree structure for force calculation. They updated the tree structure at every ~ 10 steps for the problem they showed in their paper.

In this paper, we describe a completely different method to reduce the cost of gravitational force calculation using tree with individual time-step method in SPH. The basic idea of our method is to assign different time-steps to gravitational and hydrodynamical interactions of one particle. As stated earlier, the smallest time-steps are associated with particles heated by SNe feedback. These particles have the thermal and kinetic energy many orders of magnitudes larger than the gravitational potential energy. Moreover, gravitational force changes much more slowly compared to the hydrodynamical force (pressure and artificial viscosity). Therefore, if we assign different time-steps to gravitational and hydrodynamical forces, we should be able to use much longer time-step for gravity, thereby reducing the tree construction cost by a large factor.

Our approach is similar to the multiple time-step method used in molecular dynamics, in which the long-range Coulomb force is updated less frequently than short-range van der Waals force (Streett et al. 1978). The main difference is that we combine the force splitting with individual time-steps.

The structure of this paper is as follows. In section 2, we estimate the time-steps of particles in the hot region. In

section 3, we describe our new integration method for self-gravitating fluid, **FAST** (**F**ully **A**synchronous **S**plit **T**ime-integrator). We briefly explain its implementation in §4. We present the results of test calculations and timing results in section 5. In section 6, we provide summary and discussion.

2. Estimate of Time-steps in Heated Regions

We here estimate the typical time-step of an SPH particle heated by SNe. For simplicity, we adopt following four assumptions. First, we adopt a single stellar population (SSP) approximation for a star particle with Salpeter initial mass function (Salpeter 1955) and the range of this initial mass function is set to be $0.1 M_\odot$ to $100 M_\odot$. For this initial mass function, the specific SN rate is $\epsilon_{\text{SN}} \simeq 0.0074 \text{ SN}/M_\odot$, where we assume $8 M_\odot$ or heavier stars become SNe at the final phase of their evolutions. Second, we assume that each SN injects the thermal energy of $E_{\text{SN}} = 10^{51}$ ergs to the surrounding ISM (the nearest N_{nb} particles). Third, we assume that the whole energy from SNe in a star particle discharges in a single event (this is one of SN feedback implementations proposed by Okamoto et al. 2008). Finally, we assume that the masses of the stellar and gas particles are the same.

The mean additional internal energy for N_{NB} SPH particles due to SNe of a single stellar particle is given by

$$U_{\text{SN}} = \frac{\epsilon_{\text{SN}} m_* E_{\text{SN}}}{N_{\text{NB}} m_{\text{SPH}}}, \quad (2)$$

$$\simeq 0.0074 \times 10^{51} \times \frac{m_*}{N_{\text{NB}} m_{\text{SPH}}} [\text{ergs}/M_\odot], \quad (3)$$

$$\simeq \frac{3.7 \times 10^{15}}{N_{\text{NB}}} [\text{ergs/g}], \quad (4)$$

where m_* and m_{SPH} are the masses of stellar and gas particles, respectively, and we use the relation $m_* = m_{\text{SPH}}$. The sound speed, c_{SN} , of the heated gas region is

$$c_{\text{SN}} \simeq \sqrt{\gamma(\gamma-1)U_{\text{SN}}}, \quad (5)$$

$$\simeq \frac{6.4 \times 10^2}{N_{\text{nb}}^{0.5}} [\text{km/s}], \quad (6)$$

where we assume an ideal gas with the adiabatic index of $\gamma = 5/3$. The original internal energy of the ISM before SNe, U_{ISM} , is quite small, therefore we neglected U_{ISM} in the estimation of c_{SN} . The size of an SPH particle, λ , is

$$\lambda = \left(\frac{3}{4\pi} \frac{m_{\text{SPH}}}{\rho} \right)^{1/3}, \quad (7)$$

where m_{SPH} and ρ are the mass and density of the SPH particle. Combining equations (6) and (7), we obtain the sound crossing time, $t_{\text{SN}} \equiv \lambda/c_{\text{SN}}$, in the heated region as follows:

$$t_{\text{SN}} \simeq 4 \times 10^4 \left(\frac{m_{\text{SPH}}}{1000 M_\odot} \right)^{1/3} \left(\frac{100 \text{ cm}^{-3}}{N_{\text{H}}} \right)^{1/3} [\text{yr}], \quad (8)$$

where we adopt $N_{\text{NB}} = 32$ and N_{H} is the hydrogen number density of the heated region. The typical time-step in the

region is $dt_{\text{SN}} \sim 0.1 \times t_{\text{SN}}$. This equation tells us that the smallest time-step in simulations involving the low temperature ISM and SNe becomes shorter when mass resolution becomes higher and injected region becomes denser.

In conventional simulations of galaxy formation, where the typical mass resolution is $10^6 M_\odot$ and the highest density of the ISM is 0.1 cm^{-3} , the typical time-step for the heated region is $dt_{\text{SN}} \sim 4 \times 10^5 \text{ yr}$. On the other hand, in state-of-the-art simulations involving the multiphase ISM, where $m_{\text{SPH}} = 10^3 M_\odot$ and $N_{\text{H}} = 100 \text{ cm}^{-3}$, the typical time-step is $dt_{\text{SN}} \sim 4 \times 10^3 \text{ yr}$. Simulations with resolution high enough to resolve the cold and dense gas and star forming regions require the time-steps about two order of magnitudes smaller compared to that required by conventional simulations of galaxy formation in which the gas cooling is halted at $T = 10^4 \text{ K}$. If we cannot handle cold gas, there is not much reason to go to high resolution, since smaller-scale structure formation is suppressed. Thus the number of particles in fully self-consistent simulations have not increased much in the last two decades.

3. Basic Idea

The basic idea of our new scheme is as follows. We allow gas (SPH) particles to have different time-steps for gravitational and hydrodynamical integrations. Thus, we extend the idea of individual time-steps, which allows different particles to have different time-steps, to allow single particle to have different time-steps for different interactions. We then asynchronously integrate gravity and hydrodynamics with these different time-steps. This is the essence of our FAST method. Since the problem we have to solve is the time-integration of very hot gas particles formed by SNe, we allow time-steps for gravity to be longer than those for hydrodynamics. To allow different time-steps for gravity and hydrodynamics, we use the technique of constructing multi-timestep symplectic integrator. We divide the Hamiltonian of a self-gravitating fluid system into a gravitational potential term and others, and integrate each part with its own time-step.

The Hamiltonian of a self-gravitating fluid system of N gas particles is expressed as

$$H = \sum_i^N \frac{p_i^2}{2m_i} + U(\mathbf{q}, \boldsymbol{\rho}, \mathbf{s}) - \sum_i^N \frac{Gm_i m_j}{q_{ij}}, \quad (9)$$

where p_i and q_i are conjugate variables of the canonical equation for particle i , m_i is the mass of particle i , U is the internal energy of fluid, which is a function of \mathbf{q} , density, $\boldsymbol{\rho}$, and entropy, \mathbf{s} . Here, \mathbf{q} , $\boldsymbol{\rho}$, and \mathbf{s} denote $(q_1, q_2, q_3, \dots, q_N)$, $(\rho_1, \rho_2, \rho_3, \dots, \rho_N)$, and $(s_1, s_2, s_3, \dots, s_N)$, respectively. Since we take into account arbitrary forms of hydrodynamical interactions, we express the internal energy for fluid as $U(\mathbf{q}, \boldsymbol{\rho}, \mathbf{s})$. The first, second, and third terms in the right hand side of equation (9) are the kinetic, internal, and gravitational potential energy of the system, respectively. The actual equations for p and s contain the contributions of non-conservative terms like artificial

viscosity and radiative cooling/heating. For simplicity, we here regard the system as adiabatic (i.e., s_i are treated as constants). Hence the internal energy term becomes the function of $(\mathbf{q}, \boldsymbol{\rho})$ and can be regarded as a potential term in the Hamiltonian.

We split the Hamiltonian into the gravitational potential term and others (see appendix 1):

$$H_{\text{hydro}} = \sum_i^N \frac{p_i^2}{2m_i} + U(\mathbf{q}, \boldsymbol{\rho}), \quad (10)$$

$$H_{\text{grav}} = - \sum_i^N \frac{Gm_i m_j}{q_{ij}}. \quad (11)$$

We then obtain the following expression of a symplectic integrator with the second-order accuracy,

$$f(t + \Delta t) \approx e^{\frac{\Delta t}{2} \{, H_{\text{grav}} \}} e^{\Delta t \{, H_{\text{hydro}} \}} e^{\frac{\Delta t}{2} \{, H_{\text{grav}} \}} f(t), \quad (12)$$

where “ $\{, \}$ ” is a Poisson bracket and Δt is a time-step. The equation (12) can schematically rewrite as follows:

$$v'_0 = v_0 + \frac{1}{2} \Delta t a_{\text{grav}}, \quad (13)$$

$$x_0 \rightarrow (\text{Hydro update}) \rightarrow x_1, \quad (14)$$

$$v'_0 \rightarrow (\text{Hydro update}) \rightarrow v'_1, \quad (15)$$

$$v_1 = v'_1 + \frac{1}{2} \Delta t a_{\text{grav}}, \quad (16)$$

where x , v , v' , and a_{grav} indicate the position, the velocity, the half-step advanced velocity, and the acceleration of gravitational force, respectively. Subscripts 0 and 1 indicate epochs of time-integration at t and $t + \Delta t$, respectively.

There are many ways to integrate the hydrodynamical part of equation (12), we here choose the second-order symplectic method (e.g., Hernquist & Katz 1989). We divide equation (10) again into the following two parts:

$$H_{\text{hydro}, \text{T}} = \sum_i^N \frac{p_i^2}{2m_i}, \quad (17)$$

$$H_{\text{hydro}, \text{U}} = U(\mathbf{q}, \boldsymbol{\rho}). \quad (18)$$

Consider the case that $\Delta t_{\text{g}} = l \Delta t_{\text{h}}$, where l is a natural number. We obtain a new expression of equation (12) as

$$f(t + \Delta t) \approx e^{\frac{\Delta t_{\text{g}}}{2} \{, H_{\text{grav}} \}} [e^{\frac{\Delta t_{\text{h}}}{2} \{, H_{\text{hydro}, \text{U}} \}} e^{\Delta t_{\text{h}} \{, H_{\text{hydro}, \text{T}} \}} e^{\frac{\Delta t_{\text{h}}}{2} \{, H_{\text{hydro}, \text{U}} \}}]^l e^{\frac{\Delta t_{\text{g}}}{2} \{, H_{\text{grav}} \}} f(t). \quad (19)$$

This equation tells us that we can reduce the computational cost of gravity if $\Delta t_{\text{g}} > \Delta t_{\text{h}}$ ($l > 1$). If we adopt $l = 1$, the integrator is the same as the standard “leap-frog” method for self-gravitating fluid.

In figure 1, we show schematic pictures of the usual leap-frog and FAST methods. For FAST, we consider the case that $dt_{\text{grav}} = 2 dt_{\text{hydro}}$. The computational cost of gravitational force in FAST becomes half of the leap-frog method in this case. In practice, the time-step ratio, l , adaptively changes.

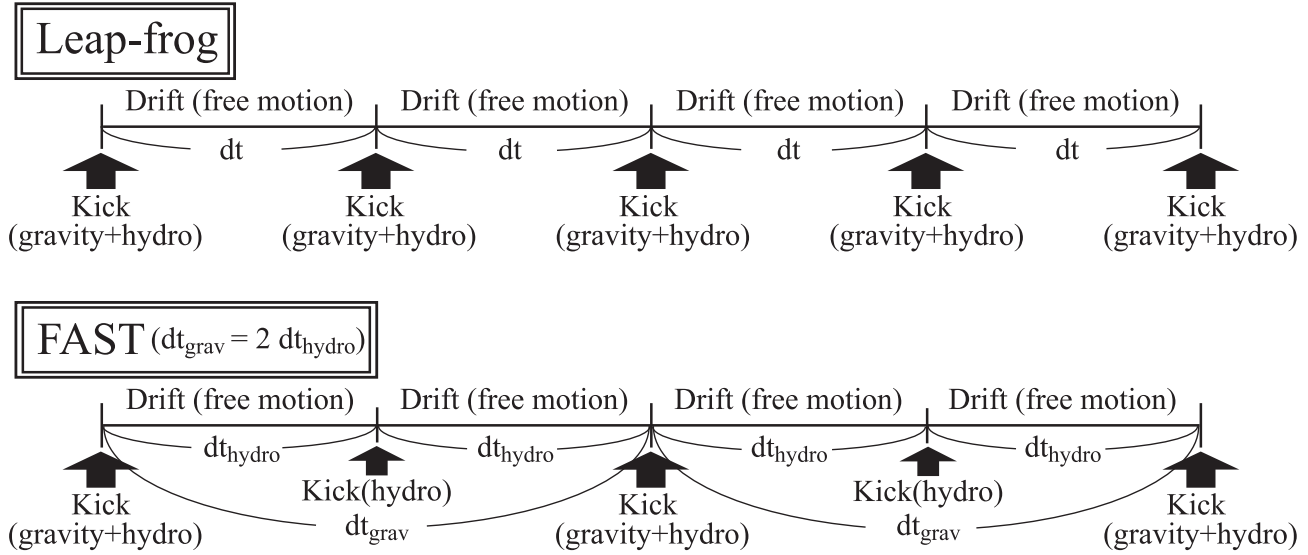


Fig. 1. The schematic picture of the leap-frog and FAST methods for the integration of a self-gravitating fluid. See also figure 1 in Fujii et al. (2007) for MVS and BRIDGE methods. “Kick” means the momentum exchanges between particles, while “Drift” denotes the free (inertial) motions under given velocity vectors.

It should be noted that, even though we borrowed the formalism of symplectic integrators to describe our FAST method, the FAST method itself is not symplectic. This is because we change the time-steps for gravitational and hydrodynamical interactions, after we split the Hamiltonian. In addition, we use different time-steps for different particles. There have been several proposed methods which can retain either symplecticness (Farr & Bertschinger 2007) or time symmetry (Makino et al. 2006) when used with the individual time-step method. However, these schemes are computationally expensive and it is not clear if the use of these schemes is worthwhile or not. In this paper, we concentrate on the traditional, non-symplectic implementation of individual time-step algorithm and its extension.

4. Implementation

4.1. The Code

The code used in this paper is a parallel tree SPH code, **ASURA**, which utilizes the special purpose hardware GRAPE (Saitoh in prep.). Gravitational force was solved by Tree with GRAPE (Makino 1991b). In this paper, we used the Phantom GRAPE library for calculations of gravity, which is a software emulator of GRAPE pipelines (kindly provided by Kohji Yoshikawa). We used an opening angle of 0.5 and only monopole moments for force calculations. Hydrodynamics was followed by the standard SPH method (e.g., Lucy 1977; Gingold & Monaghan 1977; Monaghan 1992). We used the “gather” formulation of SPH for the density estimation, whereas the “gather and scatter” formulation of SPH for the pressure gradient and the time derivation of internal energy (Monaghan 1992). We adopted the asymmetric form energy equation (e.g., Steinmetz & Mueller 1993). We iteratively determined the kernel radius of each SPH particle in every step in order to keep the number of neighbor particles, 32 ± 2 .

We used an artificial viscosity term, of which form is the same as that proposed by Monaghan (1997), in order to handle shocks. The value of the viscosity parameter, α , was set to be unity. **ASURA** adopts the variable and hierarchical time-step method (McMillan 1986; Hernquist & Katz 1989; Makino 1991a). We also implemented the time-step limiter for hydrodynamical interactions in order to maintain the difference of time-steps among neighbor particles small enough (Saitoh & Makino 2009). Here we adopted the factor of the time-step difference in neighbors, $f = 4$. The current version of **ASURA** implements two time integrators, namely the ordinary leap-frog and FAST methods.

4.2. Time-steps

The time-steps were determined as follows. The gravity time-step of an i -th particle was estimated by

$$dt_{\text{grav},i} = C_{\text{grav}} \min \left(\sqrt{\frac{\epsilon}{|\mathbf{a}_{\text{grav},i}|}}, \frac{|\mathbf{a}_{\text{grav},i}|}{|\dot{\mathbf{a}}_{\text{grav},i}|} \right), \quad (20)$$

where ϵ is a gravitational softening length, C_{grav} is a parameter which controls the accuracy (we here adopt 0.1), and $\dot{\mathbf{a}}_{\text{grav},i}$ is the time derivation of the acceleration, respectively.

Following Monaghan (1997), the hydrodynamical time-step of the i -th SPH particle was determined by

$$dt_{\text{hydro},i} = C_{\text{hydro}} \frac{2h_i}{v_{\text{sig},i}}, \quad (21)$$

where h_i is the kernel size of the SPH particle (the interaction scale is $2h_i$), $C_{\text{hydro}} = 0.25$, and $v_{\text{sig},i}$ is the local maximum signal-velocity of i -th particle defined by

$$v_{\text{sig},i} = \max_j (c_i + c_j - 3w_{ij}), \quad (22)$$

where j indicates the indices of neighbor particles, c_i and

c_j is the sound speed of i -th and j -th SPH particles and $w_{ij} = \mathbf{v}_{ij} \cdot \mathbf{x}_{ij} / |\mathbf{x}_{ij}|$ is a projected relative velocity between the SPH particles. We set $w_{ij} = 0$ if $w_{ij} > 0$.

When we use the FAST method, we asynchronously integrate gravity and hydrodynamics by the leap-frog method with different time-steps for gravity (Eq. 20) and hydrodynamics (Eq. 21). If $dt_{\text{grav}} \neq 2^n dt_{\text{hydro}}$ where n is an integer number of ≥ 0 , we change the gravitational time-step so that it satisfies the above criterion in the following way: we reduce the time-step of gravity to dt'_{grav} , where $dt_{\text{grav}} \geq dt'_{\text{grav}} = 2^n dt_{\text{hydro}}$, and n is the maximum integer number that satisfies this relation. If $dt_{\text{grav}} < dt_{\text{hydro}}$, we reduce dt_{hydro} to the same value as dt_{grav} .

When we used the ordinary leap-frog method, we picked up the smaller one of the two time-steps as the time-step of an SPH particle,

$$dt = \min(dt_{\text{grav}}, dt_{\text{hydro}}), \quad (23)$$

and synchronously integrated both gravity and hydrodynamics. In general, the acceleration and its differential terms in equation (20) should be measured relative to the total acceleration (i.e., the sum of the gravitational and hydrodynamical accelerations). However, in the hydrodynamical simulations, the Courant condition leads the smaller time-step compared with the time-step obtained by the total acceleration. Therefore the simple determination by equation (23) worked sufficiently.

5. Numerical tests

We performed three tests. The first test was the collapse of a gas cloud and the second test was the expansion of a gas cloud. The third test was a more realistic simulation. We performed simulations of galaxy-galaxy collisions, where galaxies consist of dark matter, star and gas particles. These tests incorporated both gravity and hydrodynamics and were representative of the evolution of self-gravitating fluid in galaxy formation simulation or other astrophysical simulations. We, hereafter, denote the results with the ordinary individual time-step method as “Ind” and the results with the individual time-step with the FAST method as “FAST”, in tables and figures. The first two tests were designed as simple tests for the validity of the FAST method, while in the third test we investigated the actual gain in the calculation speed as well as the accuracy of the result.

The first and second tests were done on a system with a 2.4 GHz Opteron 280 processor (Italy core), while the third test was done on 2.2 GHz quad-core Opteron processors (Barcelona core) of Cray XT4 system at Center for Computational Astrophysics of National Astronomical Observatory of Japan. We used one CPU core for the first and second tests, whereas we used 128 CPU cores for the third test.

5.1. Test I: Three dimensional self-gravitational collapse tests

We performed the integration of three-dimensional spherical collapse of adiabatic gas (e.g., Evrard 1988; Hernquist & Katz 1989). This test is one of standard tests for SPH method which involves self-gravity.

We prepared a gas sphere with the total mass and the radius both unity. The gravitational constant was also set to be unity. The initial profile of the gas sphere was $\rho(r) \propto 1/r$, where r is the distance from the center of coordinates. The adiabatic index and the specific internal energy of the gas were set to be $\gamma = 5/3$ and 0.05, respectively. The gas sphere had a negative value of the total energy, $E \sim -0.6$. When the evolution starts, the sphere begins to collapse. The shock takes place in the central region and it propagates outward. Finally, the system reaches the state of virial equilibrium. In this test, we used 30976 particles for the sphere and we followed the evolution of the gas sphere to $T = 3$. We adopted 0.038 for the gravitational softening length.

Figure 2 shows radial profiles of density, pressure, and radial velocity in three different epochs, $T = 0.9, 1.2$ and 2.4, for both the ordinary individual time-step and FAST methods. In this figure, we plotted mean physical quantities of every 300 particles. It is obvious that the results of two methods are identical. We also confirmed that these results agree well with the result obtained using global time-steps. Therefore we can conclude our new method is accurate enough.

Figure 3 shows the values of time-steps for gravity and hydrodynamics for the run with the FAST method as a function of the distance from the center at $T = 0.9$. Time-steps for gravity and hydrodynamics are different in the post-shock region and the same in the ambient, pre-shocked region. The transient region clearly matches with the shock front at the radius of ~ 0.2 (see the top-left panel of figure 2). The values of dt_{hydro} and dt_{grav} in the post-shock region differ by a factor up to four. Figure 4 shows cumulative fractions of dt_{hydro} and dt_{grav} for the simulation with the individual time-step with FAST. We can see that almost half of the particles have hydro time-steps smaller than the minimum time-step for the gravity.

The errors of the total energy, the difference between the values of the total energy at the initial ($T = 0$) and final ($T = 3$) states, for the Ind and FAST methods are shown in table 1. E_s and E_f represent the initial ($T = 0$) total energy and the final ($T = 3$) total energy, respectively. These values are acceptably small. In our test runs, the absolute value of the energy error for the time integration with FAST is smaller than that for the time integration without FAST even though the time-step for gravity is larger. The errors caused by the gravitational and hydrodynamical integrations had the opposite signs and partially canceled each other.

In table 2, we show timing results of the collapse test. Our new method is faster than the original method, but not by a large factor. The calculation time of gravity is reduced to two thirds, and that of tree construction is

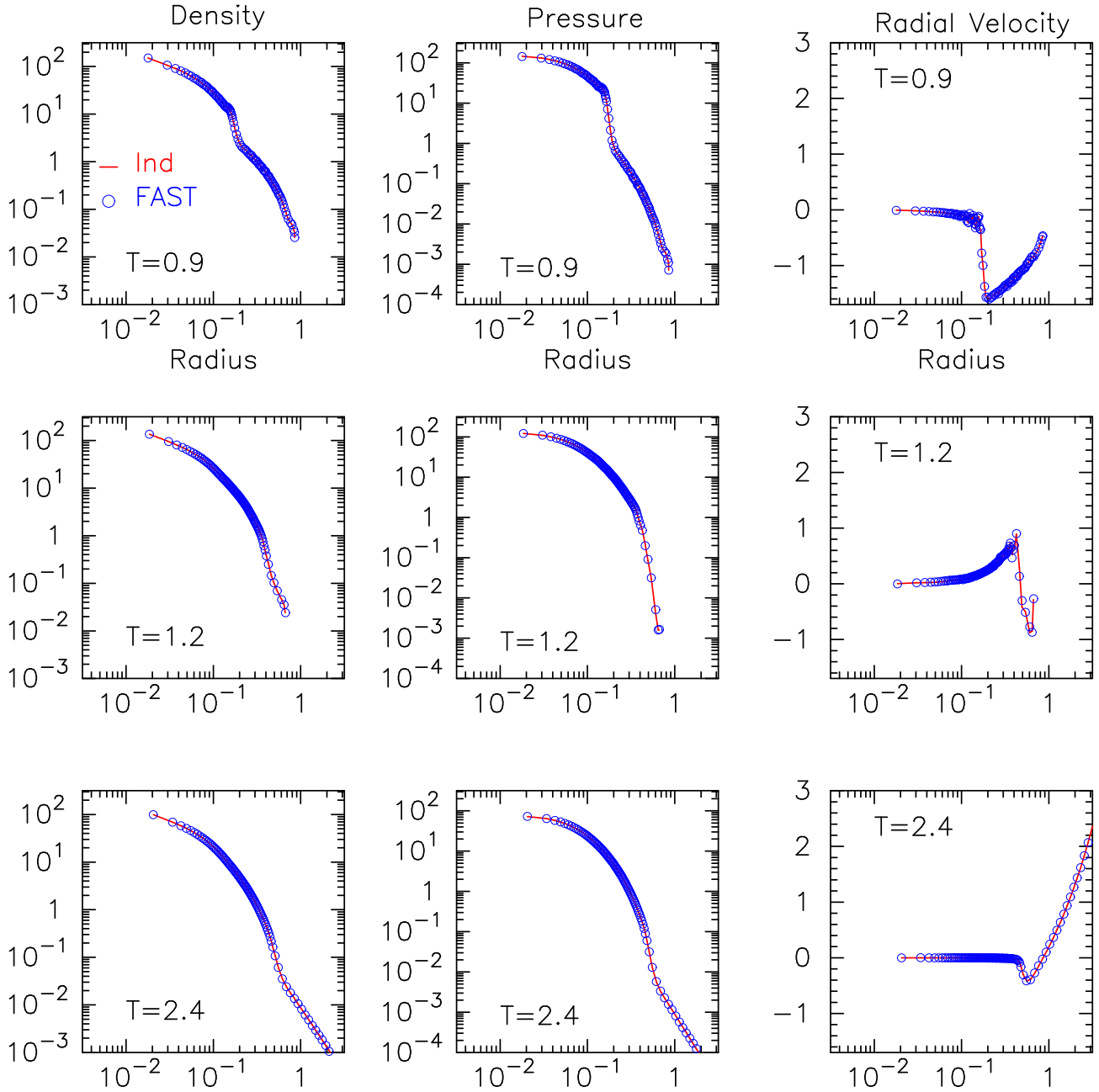


Fig. 2. Radial profiles of density (left), pressure (mid), and radial velocity (right) at $T = 0.9, 1.2$, and 2.4 (top to bottom). Horizontal axis is the distance from the origin of coordinates. Curves and circles indicate the profiles obtained with the individual and synchronous time-steps for gravity and hydrodynamics, “Ind”, and the individual and asynchronous time-steps for gravity and hydrodynamics, “FAST”.

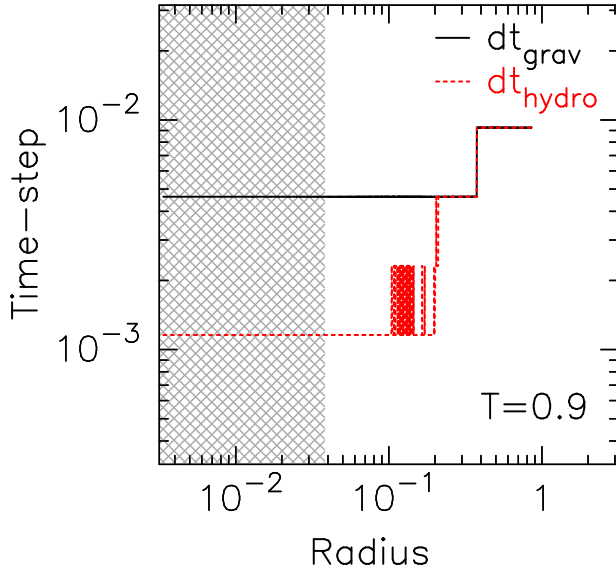


Fig. 3. Radial profiles of dt_{hydro} and dt_{grav} for the spherical collapse test with the individual time-step with FAST. The epoch is $T = 0.9$. Solid and dotted curves indicate dt_{grav} and dt_{hydro} , respectively. The hatched region corresponds with the soften region for the particle at the center by the gravitational softening.

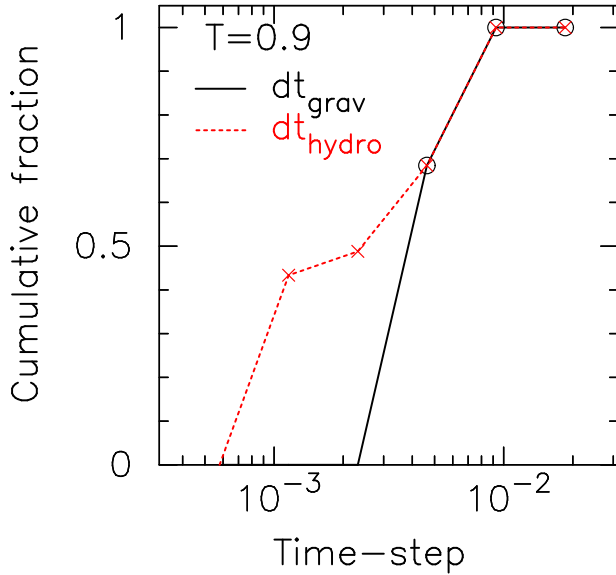


Fig. 4. Cumulative fractions of particles as a function of dt_{hydro} and dt_{grav} for the spherical collapse test with the individual time-step with FAST. The epoch is $T = 0.9$. Solid and dotted lines indicate cumulative fractions of dt_{grav} and dt_{hydro} , respectively.

Table 1. Total energy errors for the spherical collapse test.

Method	$ (E_s - E_f)/E_s $
Ind	3.0×10^{-3}
FAST	1.3×10^{-3}

Table 2. Timing results for the spherical collapse test.

Method	Time [sec]			
	Total	Gravity ^a	Hydro	Others
Ind	1754	682 (52)	960	112
FAST	1523	468 (20)	943	112

^a The tree structure construction times in the gravity part are shown as parenthetical numbers.

Table 3. Steps and the number of integrated particles for the spherical collapse test.

Method	Gravity		Hydro	
	steps	$N_{\text{int,grav}}$	steps	$N_{\text{int,hydro}}$
Ind	1979	2.4×10^7	1979	2.4×10^7
FAST	778	1.7×10^7	2022	2.4×10^7

reduced to two fifths. However, in this test the hydrodynamics part dominates the total cost.

Table 3 shows the number of steps and integrated particles for the collapse test. The ordinary individual time-step method required 1979 steps for the simulation in our implementation. The FAST method required 2022 steps for the hydrodynamics part and 778 steps for the gravity part. The reduction of the calculation time for tree construction is directly proportional to the reduction of gravity steps. In our new method, the total number of integrated particles for the gravity part becomes almost two thirds of that for the hydrodynamics part in this test.

5.2. Test II: Three-dimensional expansion tests

In this section, we describe the result of three-dimensional expansion tests. We used the particle distribution of the three-dimensional collapse test at $T = 3$ as the initial particle distribution of this expansion test. In order to let the cloud expand, we added the thermal energy in the central 32 particles with SPH manner. The total energy of the system was set to be $E = 0.5, 1, 2$, and 10. We set T to zero before the first step of the expansion calculation and follow the evolution to $T = 5$. In this test, we also plot the results of the global time-step case.

Figure 5 shows snapshots of the expanding cloud, for the case of $E = 2$, obtained with the FAST method at six different epochs ($T = 0, 1, 2, 3, 4$ and 5). The particles in the region $|z| < 0.1$ are shown in this figure. The initially compact gas cloud expands driven by the high pressure gas added in the center of the cloud, and forms a spherical shell-like structure. The shell moves outward, and at the final phase ($T = 5$), the radius of the shell becomes ~ 5 .

Figure 6 shows time evolutions of density peaks for simulations with several different values of the injection energy. The positions of peaks are derived by averaging the positions of the 10 particles with highest local density. For the reference, in this figure, we plotted the results obtained with the global-step method. There are good agreements between individual time-steps with/without FAST runs and the global time-step runs. This is because we adopted the time-step limiter for hydrodynamics

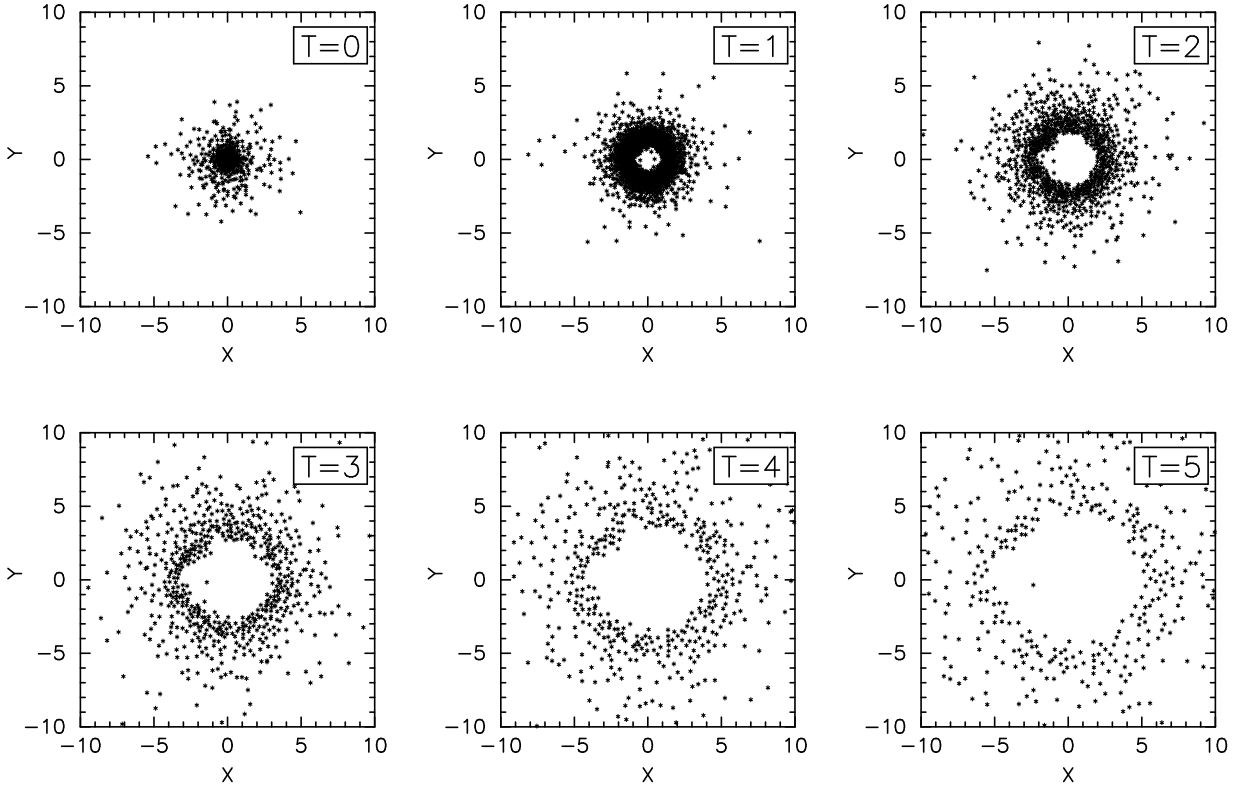


Fig. 5. Snapshots of the expanding cloud at six different epochs ($T = 0, 1, 2, 3, 4$ and 5). Projected particle distributions in a thin ($|z| < 0.1$) region are shown. Dots indicate projected particle positions. This is the case that the expansion simulation with $E = 2$. The time-integration was done by the individual time-steps with the FAST method.

(Saitoh & Makino 2009). Without this limiter, we would have failed to obtain agreements between different methods. The difference of the positions between individual time-steps with/without FAST runs are summarized in table 4. R_{Ind} and R_{FAST} represent radii of shells at $T = 5$ for individual time-step without/with FAST and global time-step runs, respectively. In the table, we also show the difference between R_{FAST} and R_{Global} , which is the radius of the shell at $T = 5$ for the global time-step runs. The difference between FAST and Ind is comparable or smaller than the difference for the result of global time-step.

Table 5 shows the timing results for the expansion test. We can see that the reduction in the cost of gravity calculation is much larger than that in the collapse test, and the reduction in the cost of tree construction is even larger. For $E = 10$, reduction in the tree construction cost is a factor of eight.

The number of integrated particles and steps are summarized in table 6. By using the FAST method, we can greatly reduce steps for the gravity part. In these simulations, the use of the FAST method resulted in the reduction of the number of gravity steps by a factor of 7 to 9. The numbers of integrated particles for the gravity part are reduced to only 0.5 – 0.7 times that of Ind runs. As is shown above, the speed up factors for the gravity part are 2.8 – 4.3. These results indicate that the decrease of the number of steps is quite efficient for integrations of

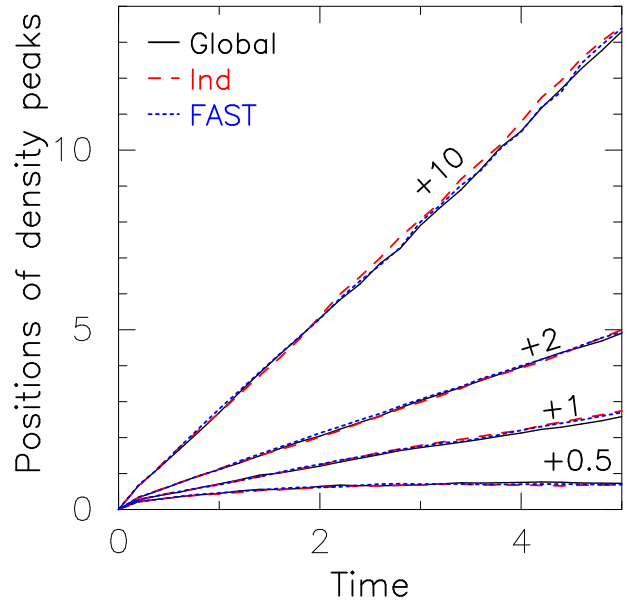


Fig. 6. Positions of density peaks as a function of time for various total energy cases. Solid, dashed, and dotted lines indicate evolutions of density peaks for cases of the global time-step (Global), ordinary individual time-steps (Ind), and individual time-steps with FAST (FAST). Numbers just above the lines indicate the values of the total energy.

Table 4. Differences between the peak positions with individual time-step with FAST and others (individual time-step without FAST and global time-step).

	$E = 0.05$	$E = 0.1$	$E = 0.2$	$E = 10$
$ \frac{R_{\text{FAST}} - R_{\text{Ind}}}{R_{\text{Ind}}} $	1.5 %	1.6 %	1.3 %	0.4 %
$ \frac{R_{\text{FAST}} - R_{\text{Global}}}{R_{\text{Global}}} $	6.4 %	6.2 %	1.9 %	1.1 %

Table 5. Timing results for cloud expansion tests.

Method	E	Time [sec]			
		Total	Gravity ^a	Hydro	Others
Ind	0.5	1264	498 (138)	550	216
FAST	0.5	972	175 (16)	568	229
Ind	1	1034	396 (100)	458	180
FAST	1	799	135 (15)	482	182
Ind	2	941	358 (92)	438	145
FAST	2	719	112 (14)	451	156
Ind	10	1018	383 (106)	466	169
FAST	10	758	89 (13)	484	185

^a Items are the same as table 3.

Table 6. Steps and number of integration particles for cloud expansion tests.

Method	E	Gravity		Hydro	
		steps	$N_{\text{int,grav}}$	steps	$N_{\text{int,hydro}}$
Ind	0.5	4675	9.0×10^6	4675	9.0×10^6
FAST	0.5	525	5.9×10^6	4431	8.8×10^6
Ind	1	3480	7.8×10^6	3480	7.8×10^6
FAST	1	479	4.8×10^6	3535	7.8×10^6
Ind	2	3515	7.5×10^6	3515	7.5×10^6
FAST	2	452	4.1×10^6	3397	7.4×10^6
Ind	10	3104	7.5×10^6	3104	7.5×10^6
FAST	10	427	3.4×10^6	3412	7.6×10^6

self-gravitating fluid. There is almost no change in the hydrodynamics part.

5.3. Test III: Merger simulations

In this section, we discuss the result of the application of the FAST method to a realistic problem, namely simulations of galaxy-galaxy collisions. Simulations we performed here were based on our recent galaxy-galaxy collision simulations of Saitoh et al. (2009), in which we followed the cooling of gas down to 10 K. We used the model of M1C. Gravity, hydrodynamics, radiative cooling, far-ultraviolet heating, star formation, and type-II SNe were taken into account. The condition for the star formation is that the gas is dense ($n_{\text{H}} > 100 \text{ cm}^{-3}$) and cold ($T < 100 \text{ K}$) with converging flows. The regions which satisfy these conditions form stars following the Schmidt-law with the local star-formation efficiency of 0.033. Further details of the modeling of star formation were described in Saitoh et al. (2008) and Saitoh et al. (2009). Gravitational softening was set to be 20 pc for all particles. The initial numbers of dark matter, (old) star, and gas particles were

6930000, 341896, and 148104, respectively. We used 128 cores of Cray XT4 system at Center for Computational Astrophysics of National Astronomical Observatory of Japan.

Figure 7 shows density and temperature maps for merger simulations at $T = 420 \text{ Myr}$ by individual time-steps without and with the FAST method. We can easily see that these two integration methods show quite similar results in density and temperature structures. The positions of “Heat spots” due to SNe are not perfectly identical because of run-to-run fluctuations. Other global properties of these galaxies are also identical for both runs.

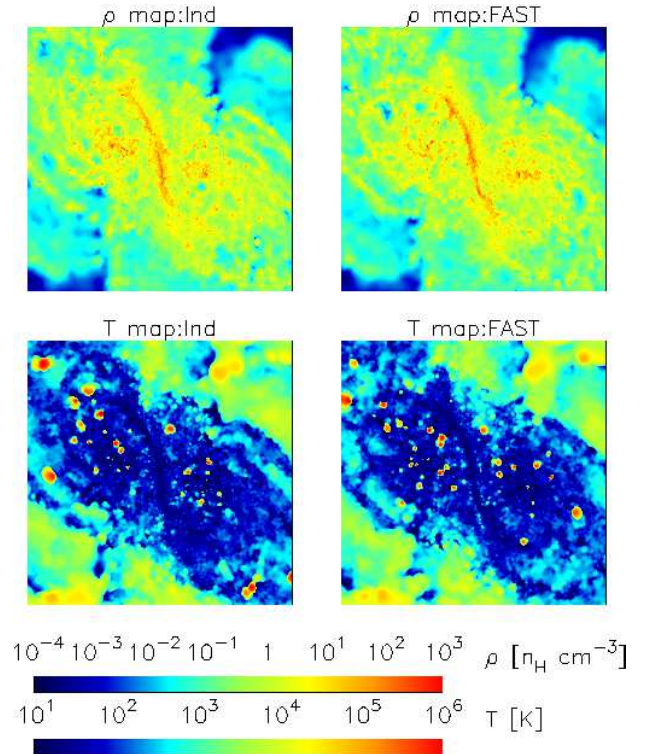
**Fig. 7.** Density and temperature maps for simulations by individual time-steps without and with the FAST method. Each panel shows $16 \text{ kpc} \times 16 \text{ kpc}$ in the orbital plane. The left and right columns show the results by individual time-steps without and with the FAST method, respectively. The epoch of these maps is $T = 420 \text{ Myr}$.

Figure 8 shows cumulative fractions of particles as a function of dt_{hydro} and dt_{grav} for SPH particles and dt_{nbody} for collisionless particles. The minimum time-step for the hydrodynamics part is shorter than that for the gravity part for SPH particles by a factor of eight. In addition, collisionless particles have longer time-steps than

SPH particles. Therefore the gravity part is skipped in the lowest 3 levels and the calculation is accelerated significantly.

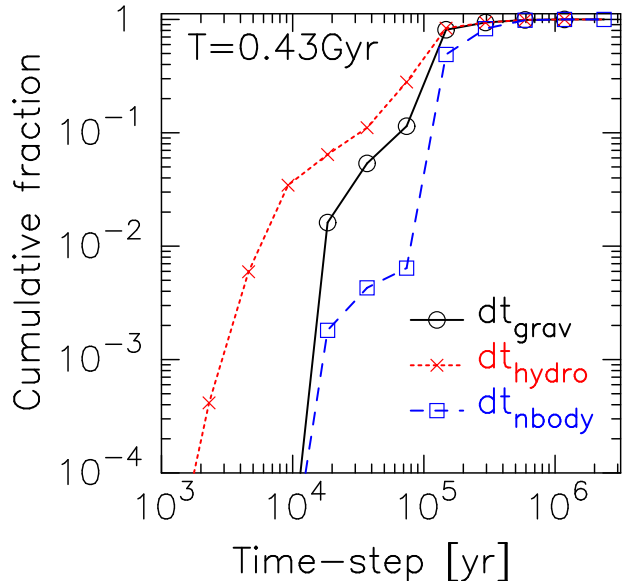


Fig. 8. Cumulative fractions of particles as a function of dt_{hydro} and dt_{grav} for SPH particles and dt_{nbody} for collisionless particles. The time-steps are sampled from the merger simulation by the individual time-step with FAST. The epoch is $T = 0.43$ Gyr. Solid, dotted, and dashed histograms indicate cumulative fractions of dt_{grav} and dt_{hydro} for SPH particles and dt_{nbody} for collisionless particles.

Table 7 shows timing results of merging simulations. We sampled two typical epochs, i.e., $350 \text{ Myr} \leq T < 400 \text{ Myr}$ and $400 \text{ Myr} \leq T < 450 \text{ Myr}$. The former epoch is a quiescent star forming phase before the first encounter while the later epoch is a significantly enhanced star forming phase during the first encounter. The total integration time for the simulation with the FAST method decreases by almost a factor of two from that of the simulation without the FAST method. With the FAST method, the gravity part is ~ 7 times faster than that without the FAST method. The reduction of the total calculation time is similar for quiescent and starburst phases.

In table 8, we show numbers of time-steps and integrated particles for gravity and hydrodynamics parts. The simulation with the FAST method required ~ 7 times smaller number of gravity steps than that without the FAST method. Note that the number of integrated particles for gravity is almost the same for the Ind and FAST method. The large reduction in the calculation time is due to both the reduction of the number of tree constructions and the removal of force calculations with small number of particles, where the calculation becomes inefficient in individual time-steps or parallel computers.

6. Summary and Discussion

We proposed a fast integrated method, “FAST”, for self-gravitating fluid. The FAST method assigns different

time-steps for gravitational and hydrodynamical interactions and integrates them asynchronously. The formulation of the FAST method is similar to the multi time-step method (Streett et al. 1978) and also regarded as an extension of “multi-step” symplectic integrators, such as mixed variable symplectic (Wisdom & Holman 1991), multiple stepsize (Skeel & Biesiadecki 1994), and the BRIDGE (Fujii et al. 2007) methods.

The approach of the FAST method is qualitatively different from other reduction techniques of the tree construction in gravity part. The FAST method eliminates unnecessary tree constructions (and gravity calculations) by adopting longer time-steps for gravitational evolution than that for hydrodynamics.

We found that the evolution of collapsing and expanding self-gravitating fluid by the FAST method are identical to these by the usual unsplit method which integrates gravity and hydrodynamics synchronously.

As a realistic test, we applied the FAST method to merger simulations including self-gravity, hydrodynamics, radiative cooling, far-ultraviolet heating, and SN (Saitoh et al. 2009). In this test, we found that simulations with and without the FAST method showed quite similar evolution. The calculation with FAST was nearly a factor of two faster. This large gain was due to the reduction in the gravity steps with small number of particles. The FAST method is very effective in accelerating simulations of self-gravitating fluid.

We thank Takashi Ito, Keiichi Wada, Michiko Fujii and Tomoaki Ishiyama for useful discussion. We also thank Kohji Yoshikawa, who kindly provided us with a custom version of the Phantom-GRAPE library. A part of numerical tests were carried out on Cray XT4 and GRAPE system at Center for Computational Astrophysics of National Astronomical Observatory of Japan. This project is supported by Grant-in-Aid for Scientific Research (17340059) of JSPS, MEXT Japan the Special Coordination Fund for Promoting Science and Technology, “GRAPE-DR Project”, and Molecular-Based New Computational Science Program of NINS. TRS is financially supported by a Research Fellowship from the Japan Society for the Promotion of Science for Young Scientists.

Appendix 1. Symplectic integration method and its variants

In this appendix, we explain the symplectic integration method briefly. Then we explain sophisticated versions of symplectic integration methods, i.e., mixed variable symplectic method (Wisdom & Holman 1991), multiple stepsize method (Skeel & Biesiadecki 1994), and the BRIDGE (Fujii et al. 2007) methods.

Symplectic integration methods (e.g., Dragt & Finn 1976; Forest & Ruth 1990; Yoshida 1990; Yoshida 1993) are now widely used in the simulations of gravitating N -body systems. These methods preserve the symplectic

Table 7. Timing results for merger simulations.

Method	Epoch	Time [sec]			
		Total	Gravity ^a	Hydro	Others ^b
Ind	350 Myr → 400 Myr	14301	5887 (2132)	3545	4869
FAST	350 Myr → 400 Myr	7249	919 (264)	2923	3407
Ind	400 Myr → 450 Myr	16454	6703 (2441)	4041	5710
FAST	400 Myr → 450 Myr	9646	953 (279)	4152	4541

^a Items are the same as table 3. ^b In this test runs, “Others” includes the calculation times of the radiative cooling, star formation, and SNe routines.

Table 8. Steps and number of integrated particles for merger simulations.

Method	Epoch	Gravity		Hydro	
		steps	$N_{\text{int,grav}}$	steps	$N_{\text{int,hydro}}$
Ind	350 Myr → 400 Myr	18697	1.6×10^9	18697	5.8×10^7
FAST	350 Myr → 400 Myr	2310	1.6×10^9	16626	6.4×10^7
Ind	400 Myr → 450 Myr	21296	1.8×10^9	21296	7.3×10^7
FAST	400 Myr → 450 Myr	2425	1.8×10^9	22959	8.0×10^7

form of the canonical equation of motions when calculating the time variation of the system. This character leads to the very good conservation of system’s total energy on the course of numerical calculation.

When we express H as the Hamiltonian of the system, and p and q as six-dimension coordinates, canonical equations are

$$\frac{dq}{dt} = \frac{\partial H}{\partial p}, \quad (\text{A1})$$

$$\frac{dp}{dt} = -\frac{\partial H}{\partial q}. \quad (\text{A2})$$

We can summarize above two equations as

$$\frac{df}{dt} = \{f, H\}, \quad (\text{A3})$$

where f is p or q , respectively, and $\{, \}$ is a Poisson bracket. We define an operator that

$$\{, H\}f \equiv \{f, H\}. \quad (\text{A4})$$

We can write a generalized canonical equation (A3) as

$$\frac{df}{dt} = \{, H\}f. \quad (\text{A5})$$

When we integrate equation (A5) from t to $t + \Delta t$, the formal solution of the equation (A5) is written as

$$f(t + \Delta t) = e^{\Delta t \{, H\}} f(t). \quad (\text{A6})$$

Here, we consider the Hamiltonian of a self-gravitating system with N particles. In this case, the Hamiltonian is written as

$$H = H_A + H_B, \quad (\text{A7})$$

where

$$H_A = \sum_i^N \frac{p_i^2}{2m_i}, \quad (\text{A8})$$

$$H_B = -\sum_{i < j}^N \frac{Gm_i m_j}{q_{ij}}. \quad (\text{A9})$$

The formal solution is written as

$$f(t + \Delta t) = e^{\Delta t (\{, H_A\} + \{, H_B\})} f(t). \quad (\text{A10})$$

Applying Barker-Champbell-Hausdorff formula (Varadarajan 1984) to equation (A10), we obtain a first order integrator

$$f(t + \Delta t) \approx e^{\Delta t \{, H_A\}} e^{\Delta t \{, H_B\}} f(t), \quad (\text{A11})$$

and a second order integrator

$$f(t + \Delta t) \approx e^{\frac{\Delta t}{2} \{, H_A\}} e^{\Delta t \{, H_B\}} e^{\frac{\Delta t}{2} \{, H_A\}} f(t). \quad (\text{A12})$$

This second order integrator is well known as the *leap-frog* integrator.

It is widely known that symplectic integration methods can achieve high-accuracy once we split Hamiltonians into several components. Mixed variable symplectic (MVS) method (Wisdom & Holman 1991; Kinoshita et al. 1991) splits the Hamiltonian into an unperturbed part with an analytic solution (i.e., Keplerian motion when we traced planetary motion) and a perturbation part (i.e., mutual gravitational perturbation among planets). When the system is nearly integrable, the Hamiltonian for the unperturbed part becomes much larger than that of the perturbed part, which enables the method to accomplish a very high accuracy in integrating the equations of motion, compared with conventional symplectic integrators.

The multiple stepsize (MSS) method (Skeel & Biesiadecki 1994; Duncan et al. 1998) splits a potential into the sum of potentials of a short-range and a long-range forces and gives different time-steps for different ranges of forces. The MSS method accomplishes the similar accuracy compared with the usual symplectic method applied with small time-step. The use of

different time-steps for different interactions was proposed for the integration of molecular dynamics (Streett et al. 1978). **GADGET-2** (Springel 2005), which employs a TreePM method for gravitational force calculation, adopts different time-steps for the long-range force derived from a Particle-mesh method (Hockney & Eastwood 1981) and the short-range force derived from a Tree method (Barnes & Hut 1986).

BRIDGE (Fujii et al. 2007) was developed in order to solve galaxy-star cluster systems self-consistently. **BRIDGE** divides a Hamiltonian of a galaxy-star cluster system into a star cluster and a galaxy parts, and applies different time-steps and integrators. In **BRIDGE**, the integration of star cluster particles is performed by a forth-order integration method, namely Hermit method (Makino & Aarseth 1992). Force calculations among star clusters are performed by direct method with **GRAPE** (Sugimoto et al. 1990). The integration of galaxy particles is performed by the leap-frog method with the Tree method for the force estimation. Forces between star cluster particles and galaxy particles are also calculated by the Tree method with constant time-step. Therefore this method can deal with coevolution of collisionless and collisional systems self-consistently.

References

- Aarseth, S. J. 1963, *MNRAS*, 126, 223
 Barnes, J., & Hut, P. 1986, *Nature*, 324, 446
 Dragt, A. J., & Finn, J. M. 1976, *Journal of Mathematical Physics*, 17, 2215
 Duncan, M. J., Levison, H. F., & Lee, M. H. 1998, *AJ*, 116, 2067
 Evrard, A. E. 1988, *MNRAS*, 235, 911
 Farr, W. M., & Bertschinger, E. 2007, *ApJ*, 663, 1420
 Forest, E., & Ruth, R. D. 1990, *Phys. D*, 43, 105
 Fujii, M., Iwasawa, M., Funato, Y., & Makino, J. 2007, *PASJ*, 59, 1095
 Gingold, R. A., & Monaghan, J. J. 1977, *MNRAS*, 181, 375
 Governato, F. et al. 2009, *MNRAS*, 957
 Hernquist, L., & Katz, N. 1989, *ApJS*, 70, 419
 Hockney, R. W., & Eastwood, J. W. 1981, *Computer Simulation Using Particles* (Computer Simulation Using Particles, New York: McGraw-Hill, 1981)
 Katz, N., & Gunn, J. E. 1991, *ApJ*, 377, 365
 Kim, J., Park, C., Gott, J. R. I., & Dubinski, J. 2008, *ArXiv e-prints*
 Kinoshita, H., Yoshida, H., & Nakai, H. 1991, *Celestial Mechanics and Dynamical Astronomy*, 50, 59
 Lucy, L. B. 1977, *AJ*, 82, 1013
 Makino, J. 1991a, *PASJ*, 43, 859
 —. 1991b, *PASJ*, 43, 621
 Makino, J., & Aarseth, S. J. 1992, *PASJ*, 44, 141
 Makino, J., Hut, P., Kaplan, M., & Saygin, H. 2006, *New Astronomy*, 12, 124
 McMillan, S. L. W. 1986, in *Lecture Notes in Physics*, Berlin Springer Verlag, Vol. 267, *The Use of Supercomputers in Stellar Dynamics*, ed. P. Hut & S. L. W. McMillan, 156–
 McMillan, S. L. W., & Aarseth, S. J. 1993, *ApJ*, 414, 200
 Monaghan, J. J. 1992, *ARA&A*, 30, 543
 —. 1997, *Journal of Computational Physics*, 136, 298
 Navarro, J. F., & Benz, W. 1991, *ApJ*, 380, 320
 Nelson, A. F., Wetzstein, M., Naab, T., & . 2008, *ArXiv e-prints*, 802
 Okamoto, T., Nemmen, R. S., & Bower, R. G. 2008, *MNRAS*, 385, 161
 Saitoh, T. R., Daisaka, H., Kokubo, E., Makino, J., Okamoto, T., Tomisaka, K., Wada, K., & Yoshida, N. 2008, *PASJ*, 60, 667
 —. 2009, *PASJ*, 61, 481
 Saitoh, T. R., & Makino, J. 2009, *ApJL*, 697, L99
 Salpeter, E. E. 1955, *ApJ*, 121, 161
 Skeel, R. D., & Biesiadecki, J. J. 1994, *Ann. Numer. Math*, 1, 191
 Springel, V. 2005, *MNRAS*, 364, 1105
 Springel, V., Yoshida, N., & White, S. D. M. 2001, *New Astronomy*, 6, 79
 Steinmetz, M., & Mueller, E. 1993, *A&A*, 268, 391
 Streett, W. B., Tildesley, D. J., & Saville, G. 1978, *Molecular Physics*, 35, 639
 Sugimoto, D., Chikada, Y., Makino, J., Ito, T., Ebisuzaki, T., & Umemura, M. 1990, *Nature*, 345, 33
 Suto, Y., & Sugihara, T. 1991, *ApJL*, 370, L15
 Varadarajan, V. 1984, *Lie Groups, Lie Algebras and their Representations* (Springer, Berlin)
 Wadsley, J. W., Stadel, J., & Quinn, T. 2004, *New Astronomy*, 9, 137
 Wetzstein, M., Nelson, A. F., Naab, T., & Burkert, A. 2008, *ArXiv e-prints*, 802
 Wisdom, J., & Holman, M. 1991, *AJ*, 102, 1528
 Yoshida, H. 1990, *Physics Letters A*, 150, 262
 —. 1993, *Celestial Mechanics and Dynamical Astronomy*, 56, 27